Excitonic recombination dynamics in shallow quantum wells

J. Tignon,* O. Heller, Ph. Roussignol, J. Martinez-Pastor,† P. Lelong, and G. Bastard
Laboratoire de Physique de la Matière Condensée de l'Ecole Normale Supérieure, 24 rue Lhomond, F-75231 Paris Cedex 05, France

R. C. Iotti and L. C. Andreani
Istituto Nazionale per la Fisica della Materia, Dipartimento di Fisica ''A. Volta,'' Università di Pavia, via Bassi 6, I-27100 Pavia, Italy

V. Thierry-Mieg and R. Planel
L2M, 169 Avenue Henri Ravera, F-92220 Bagneux, France

(Received 13 January 1998)

We report a comprehensive study of carrier-recombination dynamics in shallow $Al_xGa_{1-x}As/GaAs$ quantum wells. At low crystal temperature (2 K), the excitonic radiative recombination time is shown to be strongly enhanced in shallow quantum wells with $x>0.01$, consistently with a model that takes into account the thermal equilibrium between the three-dimensional exciton gas of the barrier and the two-dimensional exciton gas, which are closer in energy as x decreases. Furthermore, we demonstrate the existence of a thermally activated escape mechanism due to the low effective barrier height in these structures. The nonradiative recombination is shown to dominate the carrier dynamics for temperatures as low as 10 K for $x\approx0.01$. Our experimental observations are analyzed using three different variational exciton calculations. In particular, we study the crossover from the two-dimensional to the three-dimensional behavior of the exciton, which occurs for x as low as 0.01 and affects mainly the oscillator strength, whereas the transition energies in shallow quantum wells can be calculated, to a large extent, using the same approximations as for conventional quantum wells. The peculiar behavior of the oscillator strength at the crossover to the weak confinement regime is obtained by expansion in a large basis. [S0163-1829(98)05035-8]

I. INTRODUCTION

$Al_xGa_{1-x}As/GaAs$ quantum wells (QW's) with very low Al concentration, known as shallow quantum wells (SQW's), have been shown to be of considerable interest, mostly for their promising application potential,[1–7] but also from a fundamental point of view.[8–13] Originally, SQW's were developed in order to increase the switching speed of electro-optic devices such as self electro-optic effect devices, photodetectors, or optical logical gates.[14–16] This is achieved by reducing the QW barrier height, which tends to reduce the carrier escape time out of biased quantum wells and allow one to increase the operating light intensity. Indeed, room-temperature excitons have been observed by electroabsorption in SQW's with x of the order of 0.01,[3] whereas the carrier escape time, studied by pump-probe,[1] four-wave-mixing,[2] and photoluminescence experiments,[7] has been shown to be very short even for very low applied electric fields. More fundamentally, SQW's present the interesting case of intermediate confinement, where both the two-dimensional (2D) (conventional QW's) and 3D (bulk) pictures break down. In the 2D limit (strong confinement regime), the exciton binding energy is much smaller than the confinement energy: Electrons and holes can be considered as confined independently in the direction of the QW growth, whereas in the 3D limit the particles are strongly correlated and the relative motion has to be defined in all directions. Fritze *et al.*[9] have shown how a transition between these two regimes can be induced in SQW's by application of a magnetic field. More recently, Iotti and Andreani[13] demonstrated theoretically that such a transition, in narrow or shallow QW's, is characterized by a minimum of the excitonic oscillator strength at the crossover between the two regimes. This property must have some important consequences on the recombination dynamics in SQW's since the excitonic radiative recombination rate is proportional to the excitonic oscillator strength.[17] Moreover, this problem deserves some clarification since after excitation of excitons or electron-hole pairs, dephasing mechanisms,[18] or thermalization via interaction with acoustic phonons,[19] lead to an intricate dynamics in which the effect of the oscillator strength variation is difficult to predict. Additionally, an important amount of work, both theoretical and experimental,[20,21] has been devoted to carrier capture by QW's and SQW's.[22] This issue is important, for instance, in terms of efficiency for photonic devices (e.g., laser diodes). Nevertheless, as far as applications are concerned, another mechanism is at least as relevant: carrier nonradiative recombination, which governs the recombination dynamics at room temperature. Among the various existing nonradiative recombination processes, one can distinguish between extrinsic and intrinsic ones. On the one hand, nonradiative recombination can occur on crystal defects or impurity centers[23] in low-quality samples. On the other hand, nonradiative recombination can be thermally activated, even in high-quality samples, when the thermal energy is large enough for carriers to escape the QW's. Thermally activated carrier escape has been previously studied by continuous-wave (cw) photoluminescence (PL) and by time-resolved photoluminescence (TRPL), in $In_yGa_{1-y}As/GaAs$ QW's (Refs. 24–26) or thin $Al_xGa_{1-x}As/GaAs$ QW's.[27]

In this article we report on carrier recombination dynamics in a set of eight high-quality $Al_xGa_{1-x}As/GaAs$ quantum wells, with x varying between 0.006 and 0.18, hence ranging from shallow quantum wells to conventional, deep, quantum wells, studied by means of cw PL and TRPL for temperatures between 2 K and room temperature. At low temperature we observe a strong enhancement of the excitonic radiative recombination time in SQW's, with a maximum around $x=0.015$. This behavior cannot be related to the variation of the excitonic oscillator strength and is discussed with the help of a simple model taking into account the increasing role played by barrier excitons as x decreases. Additionally, we show that thermal escape of carriers out of the well is activated for increasing temperature. In order to obtain better insight of the problem, we analyze our experimental observations with three different variational calculations. First, we use an approximation known to hold for deep QW's: The exciton wave function is separable in the QW plane and the growth direction. Such an approximation fails when the confinement energy tends to zero, leading to a low estimate of the excitonic binding energy. Nevertheless, a comparison with the results obtained with a nonseparable wave function (which gives more correctly the exciton binding energy in the 3D limit) and via diagonalization of the Hamiltonian on a large nonorthogonal basis[13] allows a more quantitative discussion. We show that all three methods provide a good estimate of the optical transition energies for x values as low as 0.01 (in 100-Å-wide QW's) and that the main inaccuracy remains the neglect of the coupling between the valence subbands.

This article is organized as follows. In Sec. II we present the theoretical framework underlying our analysis. In Sec. III, after describing the samples and experiments, we discuss the validity of the calculations presented in Sec. II. Section IV is devoted to cw PL results, in particular versus excitation density, which shows the existence of a nonradiative channel whose microscopic origin is revealed by TRPL. TRPL results are discussed in Sec. V. We discuss first the radiative recombination time, measured at low temperature and then the nonradiative recombination dynamics.

II. THEORETICAL FRAMEWORK

We first apply the variational calculation previously described in Ref. 22. Considering that the in-plane center-of-mass motion ($\mathbf{R}_{xy}$) and relative motion ($\mathbf{r}_{xy}$) of the electron-hole pairs are decoupled, the eigenwave vectors of the system Hamiltonian can be written

$$\Psi(r_e,r_h)=N\ \exp(i\mathbf{K}_{xy}\cdot\mathbf{R}_{xy})\Phi(z_e,z_h,\mathbf{r}_{xy}). \tag{1}$$

In a first approximation, we consider that (i) the Coulomb interaction does not modify the single-particle confinement energy along the growth direction (Oz) and (ii) the confinement is strong enough so that the exciton does not propagate along z. In the envelope function approximation, the first trial $1s$ exciton wave function is then separable in z (growth direction) and x-y (QW plane) directions:

$$\Phi(r_e,r_h)=\chi_e(z_e)\chi_h(z_h)\beta(\mathbf{r}_{xy}), \tag{2}$$

$$\beta(\mathbf{r}_{xy})=\sqrt{2/\pi\lambda_{2D}^2}\ \exp(-\mathbf{r}_{xy}/\lambda_{2D}), \tag{3}$$

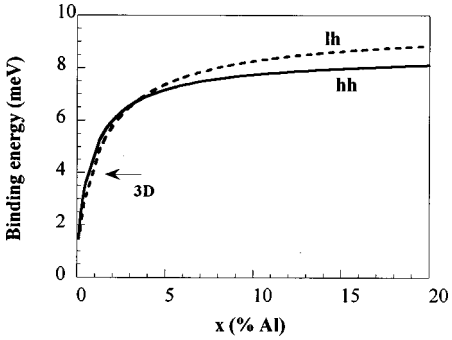

FIG. 1. $1s$, $n=1$, exciton binding energy for the light-hole exciton (dashed line) and heavy-hole exciton (solid line), calculated using the separable wave-function approximation, as a function of the Al concentration.

where χ_e (χ_h) is the solution of the one-dimensional finite quantum-well potential for the electron (hole) and ϕ depends only on the electron-hole relative motion in the QW plane. λ_{2D} is the only variational parameter, giving the effective, 2D Bohr radius. We assumed parabolic, uncoupled valence and conduction bands. For the band discontinuities we used the recent experimental results by Yu *et al.*[28]

For comparison with temperature-dependent photoluminescence measurements, we define the effective barrier height Δ as

$$\Delta_{e,h}=E_{e,h}^b-E_{e,h}, \tag{4}$$

where E_e^b (E_h^b) is the barrier potential for the electrons (holes), as given by Ref. 28, and $E_{e,h}$ are the calculated single-particle confinement energies. The effective barrier height Δ is calculated (see Fig. 11) for the electrons (solid line), heavy holes (short dashed), and light holes (long dashed), for a 100-Å QW, as a function of the Al concentration in the barrier. Above about $x=0.025$ the highest effective barrier height is for the electrons. In this region, the deeper QW potential dominates the opposite influence of the smaller mass compared to the heavy holes. This behavior is reversed for lower concentrations.

Figure 1 presents the exciton binding energy for the $n=1$, $1s$ light-hole (dashed line) and heavy-hole (solid line) excitons. As already discussed in Ref. 22, the exciton binding energy decreases for shallower quantum wells due to the reduced confinement energy together with an increase of the excitonic Bohr radius. The limitation of this first variational approach appears clearly on this figure, since for x lower than 0.005, the excitonic binding energy is found to be smaller than the 3D limit. The origin of this problem in SQW's is better understood by displaying the integrated probability to find a single particle in the QW (Fig. 2). The calculated probability for light holes and electrons is quite the same, due to the similarity of their mass along the confinement axis (Oz). When the Al concentration is decreased, electrons are more easily delocalized in the QW barrier than heavy holes that have a larger mass. For very low Al concentrations, the carriers are not confined enough in the QW plane to consider the exciton as a 2D system and the full electron-hole distance (z_e-z_h) has to be taken into account in the Coulomb exponential term of Eq. (3).

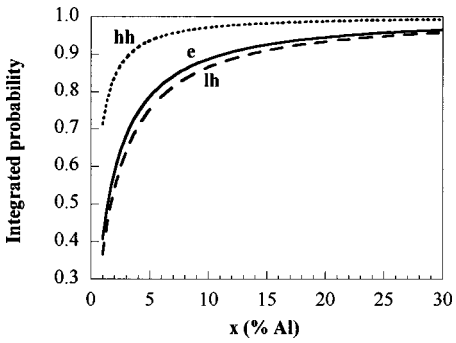

FIG. 2. Integrated probability for the heavy-hole (short-dashed line), light-hole (long-dashed line), and electron (solid line) to be in the QW layer, as a function of the Al concentration.

In order to solve the problem mentioned above we have considered, in a second approximation, the result of a variational calculation using a nonseparable wave function. This type of wave function is well adapted to calculate the exciton binding energy in a bulk material.[29] In this case, the trial function is given by

$$\Phi(r_e,r_h)=\chi_e(z_e)\chi_h(z_h)\exp[-\sqrt{\mathbf{r}_{xy}^2+(z_e-z_h)^2}/\lambda_{2D}]. \tag{5}$$

Finally, the exciton binding energy has been calculated by using the real-space expansion method described in Ref. 13. The excitonic Hamiltonian is written in the framework of the effective-mass approximation and diagonalized on a large nonorthogonal basis of Gaussian functions for all coordinates z_e, z_h and exponential ones for r_{xy}. This method is equivalent to keeping all discrete and continuum single-particle levels in the exciton; it makes no assumptions about the form of the exciton wave function and therefore allows one to describe both the strong and the weak confinement regimes as the well width or the barrier height is varied.

In Fig. 3 we compare the $1s$, $n=1$, heavy-hole exciton binding energies, calculated using a separable wave function (dashed line), using a nonseparable wave function (solid line) and the results of the more elaborate numerical calculations (dots). The second and third methods indeed allow one to calculate the correct exciton binding energy in the 3D limit (4 meV). For an Al concentration as low as 0.01, the binding energy is at least 5.3 meV, which represents an increase of as much as 33% compared to the 3D limit. Such an increase of the exciton binding energy in SQW's can be attributed to the confinement of the particles already effective for very low Al concentrations. For $x=0.01$, the integrated probability to find the heavy holes in the QW is 71% and 41% for the electrons ($n=1$ states). For higher Al concentrations, all three methods agree well. We want to stress that the discrepancies between the three methods remain smaller than 0.5 meV (our experimental precision, as discussed in Sec. III) for concentrations as low as 0.01 and higher. For $x=0.006$, which corresponds to the shallowest quantum well we have studied, the discrepancy is no more than 1 meV. Further comparison with experiment and discussion about the approximation of uncoupled valence bands are presented in Sec. III.

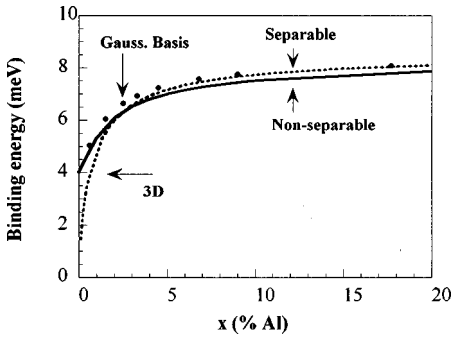

FIG. 3. $1s$, $n=1$, exciton binding energy for the heavy-hole exciton as a function x, calculated using the separable wave-function approximation (dashed line), the nonseparable wave-function approximation (solid line), or a Gaussian basis (symbols).

Finally, the excitonic oscillator strength has also been calculated using the first and third methods presented above (the inverse of the oscillator strength is plotted in Fig. 8 in the frame of the discussion presented in Sec. V B). In the separable wave-function approximation, the oscillator strength decreases monotonically with decreasing x, due to the increase of the exciton Bohr radius and to the larger penetration of the wave functions into the well barriers for shallower QW's. However, this method is known to fail for low Al concentrations and the comparison with a more sophisticated method shows that the error on the oscillator strength is even larger than the error on the energies, as expected. As discussed extensively in Ref. 13, the crossover from the strong to weak confinement regime is only obtained by an expansion in a large basis (third method). In the strong confinement regime (conventional QW's), the electron and holes can be considered as separately confined into the well. In this regime, a reduction of the barrier height or an increase of the well width leads to a decrease of the oscillator strength. On the contrary, in the weak confinement regime, i.e., when the QW can be considered as only a perturbation to the bulk 3D exciton, the exciton center-of-mass motion is quantized as a whole and the oscillator strength increases versus the well width or decreases versus the barrier height. As a consequence, a minimum of the oscillator strength is predicted, as it can be seen in Fig. 8, at the crossover between the two regimes. The predicted crossover between the two regimes occurs at $x=0.01$ for our structures and leads to a minimum of the oscillator strength for this concentration.

III. EXPERIMENT: DISCUSSION

A set of eight samples were grown by molecular-beam epitaxy on an n^+-type GaAs substrate (Si doped, 2×10^{18} cm^{-3}) and GaAs buffer, along the $\langle001\rangle$ direction. At the center of the intrinsic zone is a nominally 100-Å-wide GaAs quantum well clad with two 500-Å-wide $Al_xGa_{1-x}As$ barriers with x ranging from 0.006 to 0.178. The 1100-Å-thick structure was embedded between two 20-Å-wide AlAs layers in order to monitor the PL of both the SQW and the $Al_xGa_{1-x}As$ barrier when necessary. On top of each sample a 100-Å-thick undoped GaAs cap layer was grown. The samples were immersed in a helium cryostat allowing the temperature to vary between 2 and 300 K. Continuous-wave PL and PL excitation (PLE) spectra were excited with an Ar^+-pumped tunable Ti-sapphire cw laser. The PL signal

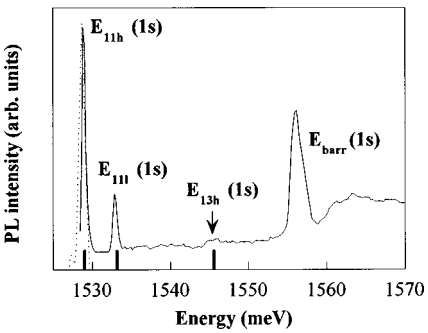

FIG. 4. Photoluminescence (dashed line) and PL excitation (solid line) for 95L19 ($x=0.033$). The vertical lines below the spectrum represent the transition energies calculated using the separable wave-function approximation.

was dispersed by a 80-cm double monochromator and detected with a cooled GaAs photomultiplier. Time-resolved photoluminescence measurements have also been performed using a synchronously pumped mode-locked Ti-sapphire laser with a 2-ps pulse duration. In this case, the signal was detected after filtering by a 32-cm double monochromator and by a streak camera system with a time resolution of $\approx$15 ps. In cw excitation the lowest excitation power was 0.1 W cm^{-2}, corresponding to a carrier density of about 10^7 cm^{-2}. In the TRPL experiments, the lowest excitation intensity corresponds to a carrier density of about 10^9 cm^{-2}.

As an example, we report in Fig. 4 the PL spectrum (dashed curve) and the PLE spectrum (solid line) for the sample 95L19 ($x=0.033$), at low excitation density and 2 K. The PL spectrum displays an intense peak at 1529 meV with a full width at half maximum (FWHM) of 1 meV. Along with this very small FWHM no Stokes shift was measured, showing the high quality of the sample. In fact, only one sample (K411, $x=0.09$) revealed a 1-meV Stokes shift and 3.8 meV FWHM for the PL, whereas a FWHM of 1 meV or less and no Stokes shift were measured on the other samples. A comparison with the nominal characteristics of the sample allows one to identify the peak at 1556.2 meV with the 1s exciton of the $Al_xGa_{1-x}As$ barriers, from which we could deduce an effective Al concentration $x=0.033$.[28] The numerical calculation then allows one to identify all the other transitions without ambiguity. At 1529 and 1533 meV are the 1s, $n=1$, heavy-hole and light-hole excitons [$E_{11h}(1s)$ and $E_{11l}(1s)$]. The small peak at 1545.9 meV has been identified with the $E_{13h}(1s)$ transition, as confirmed by calculations assuming an exciton binding energy of 2 meV (a reasonable value considering that the 3h level lies in the large well of our separate confinement heterostructure). The vertical lines below the PLE spectra are transitions calculated using the separable wave function. For this sample, the best agreement between theory and experiment is obtained for an effective well width of 106 Å, which represents a discrepancy of two monolayers with the nominal value.

In order to test the validity of the variational calculation using a separable wave function, we compare the measured transition energies with the theory in Table I. For each sample, the Al concentration (column 2) has been deduced following the same procedure as described above. The effective well width (column 3) is the one allowing the best fit of the data, once x is known. In the calculation, the well width is then the only adjustable parameter. In column 4 we report the measured energies for $E11h(1s)$ and column 5 displays the calculated energies. The same comparison is presented for $E11l(1s)$ in columns 6 and 7. The mean discrepancy between theory and experiment is only 0.5 meV, which is very good considering that this value is also the experimental accuracy and that it is comparable to the values reported in the literature, in particular by Simmonds *et al.*,[11] who studied the exciton binding energies in SQW's by high-resolution spectroscopy and analyzed their results using a nonseparable wave function. Furthermore, we emphasize that the absolute inaccuracy of the calculation is not correlated with the QW depth nor is the difference between the effective well width and the nominal well width. More precisely, one may introduce a relative inaccuracy by dividing the absolute discrepancy between theory and experiment by the confinement energy of the excitonic level, i.e., the energy difference between the SQW excitonic level of interest and the fundamental excitonic level of bulk GaAs. This relative inaccuracy is reported in column 8 of Table I for the first heavy-hole excitonic transition and in column 9 for the light-hole one. We obtain values of about 2% for $x=0.178$. The relative inaccuracy increases for x below 0.025 and reaches a value of about 5%. Hence, due to the strong enhancement of the binding energy in SQW's compared to the bulk material, a

TABLE I. Effective Al concentration (column 2), effective well width (column 3), energy of the $n=1$, 1s, heavy-hole exciton (column 4, experiment; column 5, theory) and of the light-hole exciton (column, 6, experiment; column, 7, theory), and relative inaccuracy as estimated in the text for the heavy-hole (column 8) and light-hole (column 9) excitonic transitions.

Sample	% (Al)	Width (Å)	$E11h(1s)$ Expt.	$E11h(1s)$ Theor.	$E11l(1s)$ Expt.	$E11l(1s)$ Theor.	$\varepsilon_r h(1s)$ (%)	$\varepsilon_r l(1s)$ (%)
36M52	0.6	100	1520.7	1520.9	1521.9	1522.1	3.5	2.9
95L18	1.5	120	1522.8	1523.2	1524.9	1525.6	5.1	7.1
JC09	2.5	100	1527.3	1527.5	1530.3	1531.1	1.6	5.2
95L19	3.3	106	1529	1528.9	1533	1533.3	−0.7	1.7
JC013	4.5	100	1532.4	1532.4	1537.3	1538	0	3.1
95L20	6.8	100	1536	1536	1542.7	1543.3	0	2.2
K411	9	85	1544.4	1543.9	1553.3	1553.7	−1.7	1.0
16M07	17.8	95	1547.3	1546.7	1557.5	1558.8	−1.8	3.1

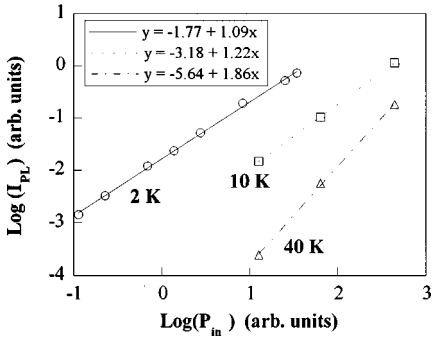

FIG. 5. Integrated photoluminescence intensity versus input power (logarithmic scales), at $T=2$ K (circles), 10 K (squares), and 40 K (triangles), for JC09 ($x=0.025$). The equations in the inset are the fit to the data.

calculation of the energies using the same approximations as for deep QW's can be applied (down to $x=0.01$, within the experimental accuracy), which is gratifying given that one might have expected the valence-band coupling to play a non-negligible role.

IV. CONTINUOUS-WAVE EXPERIMENT VERSUS EXCITATION DENSITY

Varying the excitation intensity provides a way to investigate the nonradiative recombination dynamics in QW's. The excitonic character of an observed transition can then be studied by the excitation power dependence of the PL integrated intensity. It is generally admitted that the PL-integrated intensity I_{PL} is proportional the excitation intensity I_{in} when the excitonic recombination (radiative or not) dominates. On the contrary, the PL-integrated intensity is proportional to the square of the excitation intensity when the free carrier non-radiative recombination dominates.[30,31] In an intermediate regime $I_{\mathrm{PL}} \propto I_{\mathrm{in}}^{\alpha}$, where α ranges between 1 and 2. In Fig. 5 we report the PL-integrated intensity as a function of the input power for the sample JC09 ($x=0.025$) and for three different temperatures. At low temperature, I_{PL} is indeed proportional to the excitation intensity, but in contrast to what is usually reported for QW's, α tends towards 2 (1.86 at 40 K) for unusually low temperatures. A similar behavior is observed for all SQW's. Additionally, the PL ceases to be measurable when α is close to 2. Nevertheless, the line shape of the PL lines remains exciton-like in SQW's, even when α is close to 2; we have not found any evidence of luminescence arising from dissociated electron-hole pairs.

In order to understand this behavior, we use the following model. We assume that for high temperature (a regime defined by α close to 2), the radiative recombination is essentially excitonic, as observed, but the decay of the population is dominated by the non-radiative recombination of free-electron–hole pairs. Additionally, the excitonic population and the free carriers remain in thermal equilibrium, as described by the mass action law[32]

$$\frac{np}{N}=K(T), \tag{6}$$

TABLE II. Values of α, measured for three SQW's (2.5%, 4.5%, and 9%) as a function of the temperature. The last column lists values of α in QW's with x between 0.15 and 1 (Ref. 30).

Temperature (K)	2.5%	4.5%	9%	15–100 %[a]
2	1.09	1	1	1
10	1.22	1	1.12	
40	1.86	1.38	1.14	
80		1.83	1.41	1.29–1.16
300				1.53–1.41

[a]Reference 30.

where n and p are the electron and hole densities and N the exciton density. Furthermore, the rate equation for electrons (similar for holes) can be written

$$\frac{dn}{dt}=-Bnp-\frac{n}{\tau_{\mathrm{nr}}^{e}}+g, \tag{7}$$

where B is the radiative recombination rate ($\mathrm{cm}^3\,\mathrm{s}^{-1}$), g is the creation rate, and τ_{nr}^{e} is the non-radiative recombination time for electrons. Since nonradiative recombination of free carriers dominates, one can write in the steady-state regime $n=g\tau_{\mathrm{nr}}^{e}$ for electrons and $p=g\tau_{\mathrm{nr}}^{h}$ for holes. Solving Eq. (6) then gives $N=g^2\tau_{\mathrm{nr}}^{e}\tau_{\mathrm{nr}}^{h}/K(T)$. In this model, the excitonic PL intensity is proportional to the concentration of excitons N and thus found to be proportional to g^2, i.e., to the square of the excitation density.

In Table II we report α measured for three SQW's, as a function of the temperature, as long as the photoluminescence can be measured. In the last column is reported the values of α measured by Ky *et al.*[30] in various deep QW's with Al concentration ranging from 0.15 to 1. From these results, two observations can be made: (i) α increases with increasing temperature and (ii) for a given temperature, the greater the α, the shallower the quantum well. These observations and the simple model presented above strongly suggest that the nonradiative mechanism is driven by the thermal escape of free carriers out of the well. This conclusion, along with a microscopic origin of the mechanism, is confirmed by TRPL, as described in the following section.

V. TIME-RESOLVED PHOTOLUMINESCENCE

The temperature dependence of the PL decay time, measured by time-resolved photoluminescence, is reported in Fig. 6 for all samples. In order to excite all samples in the same condition, we chose to provide the excitation in resonance with the light-hole $1s$, $n=1$ exciton, which for the case of the shallowest QW ($x=0.006$) corresponds to about 1 meV above the heavy-hole exciton. Additionally, the excitation density is kept low (about 10^9 cm^{-2}) at low temperature and increased, when necessary, at higher temperature, in order to compensate for the reduction of PL intensity, due to the activation of nonradiative processes. As previously reported in the literature,[25,26,33] the decay time increases with temperature before it decreases at higher temperature. Furthermore, it appears clearly that a maximum is reached at a lower temperature in shallower QW's.

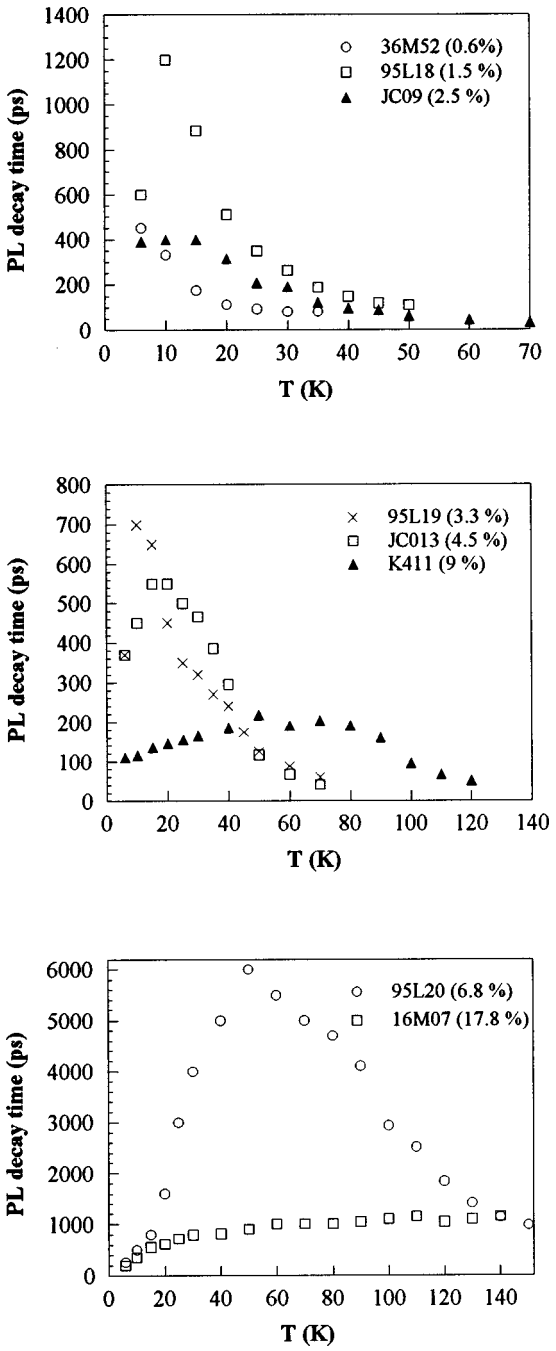

FIG. 6. Photoluminescence decay time as a function of temperature, for the complete set of samples.

A. Luminescence efficiency

The PL recombination time τ_R, identified with the decay time in our experiment, is given by

$$\tau_R^{-1}(T)=\tau_{\rm rad}^{-1}(T)+\tau_{\rm nr}^{-1}(T), \tag{8}$$

where $\tau_{\rm rad}$ is the radiative recombination time and $\tau_{\rm nr}$ is the nonradiative recombination time. The PL efficiency is then

$$\rho(T)=\frac{\tau_{\rm rad}^{-1}(T)}{\tau_{\rm rad}^{-1}(T)+\tau_{\rm nr}^{-1}(T)}. \tag{9}$$

As shown in Ref. 34, the relative variation of the radiative recombination time with temperature can be entirely deduced from the experiment by measuring the PL-integrated intensity variation and the PL decay time. Nevertheless, the absolute value of the radiative decay time requires one to know the PL efficiency at $T=0$ K since

$$\tau_{\rm rad}^{-1}(T)=\tau_R^{-1}(T)\rho(T)=\tau_R^{-1}(T)\,\frac{\rho(T)}{\rho(0)}\,\rho(0). \tag{10}$$

As previously stated, at low temperature and for high-quality samples,[35] $\rho(0)$ can be considered very close to 1, within a good approximation. Only one of our samples (K411, $x=0.09$) may not satisfy this hypothesis due to its lower quality. As an example, the PL intensity measured for JC013 ($x=0.045$) is reported in Fig. 7(a). From the steplike behavior at low temperature, it can be assumed that the recombination is essentially radiative between 0 and 15 K. The PL decay time and the radiative and nonradiative recombination times, for the same sample, are reported in Fig. 7(b), following Eqs. (10) and (8). The result for $\rho(0)=1$ is shown as a solid line and for $\rho(0)=0.9$ as a dashed line. The discrepancy between the two hypotheses remains small. Hence we will hereafter consider the two following cases: (i) at liquid helium temperature $\tau_R\approx\tau_{\rm rad}$ and (ii) at high temperature $\tau_R\approx\tau_{\rm nr}$.

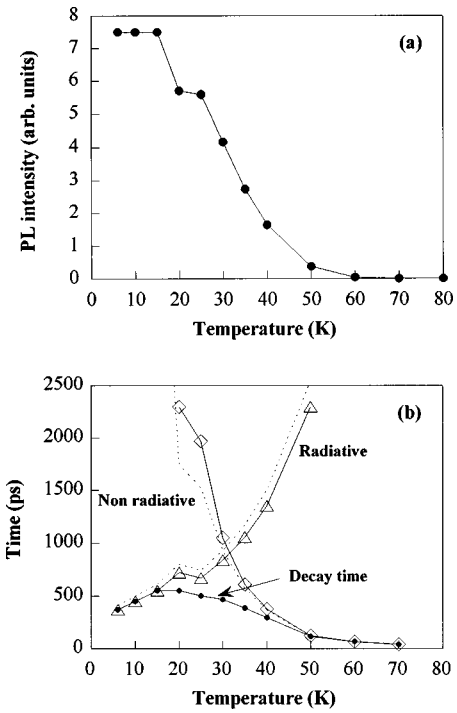

FIG. 7. (a) Photoluminescence intensity (arbitrary units) for JC013 ($x=0.045$) as a function of crystal temperature. (b) Measured photoluminescence decay time (full circles) as a function of temperature for JC013 ($x=0.045$). Triangles, deduced (see the text) radiative recombination time versus temperature, squares, deduced nonradiative recombination time.

B. Low temperature

According to the above discussion, we identify, at low temperature (2 K), the PL decay time with the radiative recombination time. The measured radiative recombination time is plotted versus the aluminum concentration in Fig. 8

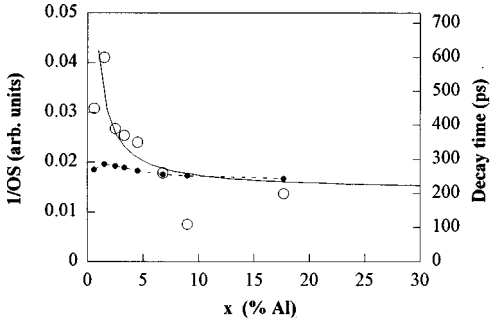

FIG. 8. Measured radiative recombination time as a function of Al concentration (open circles and right scale). Solid line, inverse of the exciton oscillator strength (arbitrary units) calculated using the separable wave-function approximation, full circles (the dashed line is a guide for the eyes), inverse of the exciton oscillator strength calculated using the Gaussian basis.

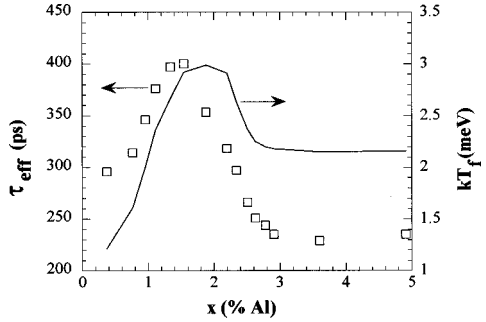

FIG. 9. Calculated radiative recombination time (symbols and left scale) and final temperature (solid line and right scale) of the QW exciton gas as a function of Al concentration. The parameters used for the calculations are given in the text.

(open symbols). The overall trend is clearly an increase from about 200 ps in an $x=0.2$ QW to about 600 ps for a SQW with $x=0.015$.

In Fig. 8 we compare the measured PL decay times with the inverse of the heavy-hole, $1s$, $n=1$ excitonic oscillator strength, as calculated by the methods described in Sec. II. In the following discussion we can discard the point at $x=0.09$ since the corresponding sample is known to be of lower quality (see above) and can experience nonradiative recombination even at low temperature. Considering the predictions of the first theoretical approach (separable wave function), the increase of the exciton radiative lifetime with decreasing Al content may at a first sight be attributed to a quantum-well property. With decreasing x the 2D aspect is lost, the QW excitons are less bound, and their oscillator strength decreases. In fact, this explanation must be rejected since our more elaborate calculations (see Fig. 8, dashed line) show that the exciton oscillator strength is essentially constant at low x.

The observed increase can be attributed to the fact that barrierlike excitons are increasingly closer in energy to the QW excitons when x decreases. These barrier excitons have a considerably larger density of states than the QW excitons. Thus, even at low crystal temperature, the barrier exciton states can be significantly populated by the initially hot exciton population. They feed the QW exciton density of states with energetic excitons that maintain the QW exciton gas at elevated temperature and thereby increase its recombination time.[36] The following simple model confirms this qualitative interpretation.

Assume that, at each time t, the QW excitons and the barrier excitons are in thermal (Boltzmann) equilibrium at a temperature $T(t)$. The real power dU/dt of the exciton gas changes because of the recombination of the QW and barrier excitons and also through exciton interactions with acoustical and optical phonons. These interactions are characterized by a relaxation time ($\tau_{\rm ac}$ and $\tau_{\rm LO}$, respectively) and a characteristic energy ($\varepsilon_{\rm ac}$ and $\varepsilon_{\rm LO}$, respectively). If we call n_X and n_B the areal densities of QW and barrier excitons, respectively, there is

$$\Psi=\frac{n_B}{n_X}=L\sqrt{\frac{MkT(t)}{2\pi\hbar^2}}\exp[-\Delta/kT(t)], \qquad (11)$$

$$U=n_B[\hbar\omega+\Delta+3/2kT(t)]+n_X[\hbar\omega+kT(t)], \qquad (12)$$

where L is the barrier length, M the total exciton mass, $\hbar\omega$ the energy of the QW excitons at the zero in-plane wave vector, and Δ the energy difference between the barrier and QW excitons. Call τ_B and τ_r the radiative lifetime of the barrier and QW excitons, respectively. Then the total exciton areal density N decreases at a rate dN/dt equal to

$$\frac{dN}{dt}=-N\,\frac{\Psi\tau_B^{-1}+\tau_r^{-1}[1-\exp(-\delta/kT_f)]}{1+\Psi}, \qquad (13)$$

where δ is the energy slice where the QW excitons can radiate (typically $\delta=0.1$ meV). In the long-time regime the excitons have thermalized to a final temperature T_f and N, as well as n_X, decreases with an effective recombination time $\tau_{\rm eff}$ given by

$$\tau_{\rm eff}^{-1}=\frac{\Psi_f\tau_B^{-1}+\tau_r^{-1}[1-\exp(-\delta/kT_f]}{1+\Psi_f}, \qquad (14)$$

where Ψ_f is the final ratio between 3D and 2D excitons. We show in Fig. 9 the calculated x dependence of kT_f and $\tau_{\rm eff}$ taking a lattice thermal energy $kT_{\rm latt}$ equal to 0.8 meV (about 9 K), $\varepsilon_{\rm ac}=1$ meV, $\varepsilon_{\rm LO}=36$ meV, $\tau_{\rm ac}=80$ ps, $\tau_{\rm LO}=1$ ps, $\tau_B=1$ ns, $\tau_r=10$ ps, $\delta=0.1$ meV, and $L=100$ nm. The exciton population is initially hot right after the excitation and for the sake of simplicity, the initial temperature is set to a constant equal to 80 K (6.9 meV) in this model. Both kT_f and $\tau_{\rm eff}$ are almost constant when $\Delta\geqslant 20$ meV ($x\geqslant 0.016$) where $\Psi\leqslant 10^{-5}$ and $\tau_{\rm eff}\approx\tau_r/[1-\exp(-\delta/kT_f)]$. We note the persistence of an equilibrium temperature T_f that is slightly larger than that of the lattice (about 24 K). This is due to the radiative recombination that suppresses the low-energy excitons and thus contributes to an effective heating of the exciton gas. The difference between T_f and $T_{\rm latt}$ increases with increasing $\tau_{\rm ac}$ and decreasing τ_r. When Δ becomes $\leqslant 20$ meV and T_f and $\tau_{\rm eff}$ increase due to the thermal proximity of the large density of states of the barrier excitons. At extremely small Δ ($\Delta\leqslant 5$ meV, $x\leqslant 0.004$) the thermalization towards lattice temperature becomes easier again because the dominant species have now become the barrier excitons ($\Psi_f=2.47$ when $\Delta=2.7$ meV, $x=0.002$). The lower equilibrium temperature in turn shortens the QW recombination

time, which leads to a decrease of τ_{eff} in spite of the fact that the QW excitons are less numerous than the barrier excitons.

The decrease of the excitonic radiative recombination time observed for the sample (of high quality) with $x=0.006$ is well reproduced by this simple model. However, other reasons may induce such a behavior. It will be shown in Sec. V C that nonradiative recombination dynamics of intrinsic origin (thermal escape out of the well) are activated in SQW's for a lower temperature in shallower wells. Consequently, in the $x=0.006$ sample, nonradiative recombination starts for a temperature as low as 10 K. Hence it can be argued that at a crystal temperature of 2 K the measured PL decay time can hardly be unaffected by these dynamics, leading to an underestimate of τ_{rad}. Another possible origin for this behavior is the crossover from strong to weak confinement regime,[13] theoretically predicted for excitons in shallow or narrow quantum wells (see Sec. II). The predicted crossover between the two regimes is calculated to take place at $x=0.01$ (Fig. 8) for our structures and induce a minimum of the oscillator strength. Note that the calculated variation of the oscillator strength is of the order of 20%, much smaller than the experimental variation of the recombination time, so that the observation of the crossover is certainly largely hindered in TRPL measurements. Thus an accurate measurement of the oscillator strength should be necessary to provide evidence of this crossover.

C. High-temperature carrier escape

We now focus on the nonradiative recombination dynamics. We have shown in Sec. IV that a nonradiative recombination channel is activated for lower temperatures in shallower QW's. In this section we show that the origin of this dynamics is the thermally activated escape of the carriers that are the less confined in the well. Following Gurioli *et al.*,[27] we choose to investigate this dynamics by studying the temperature dependence of the decay time (in the high-temperature regime) rather than by studying the PL intensity dependence. We assume the following. (i) The excitation is provided in the QW (which corresponds to the experiment). (ii) In this high-temperature regime, all the populations in the well are in thermal equilibrium with the crystal. In fact, we checked that the effective temperature deduced from the TRPL spectrum reaches the crystal temperature within 10 ps at all energies (high-temperature regime). (iii) All the populations in the PL band have the same recombination time $\tau_R \approx \tau_{\text{nr}}$, which is also verified experimentally. (iv) When the temperature is high enough, the free-carrier thermalization leads to a distribution for which the highest confined states have an energy larger than the barrier potential E_b. We then assume that the main contribution to the nonradiative dynamics comes from the scattering of these carriers towards the barrier states, with a scattering rate Γ. (v) The carriers that escaped out of the well can recombine radiatively or nonradiatively in the $Al_xGa_{1-x}As$ barrier.

It follows[27] that the nonradiative recombination time is given by

$$\tau_{\text{nr}}=\frac{1}{\Gamma\ \exp(-\Delta/k_bT)}, \tag{15}$$

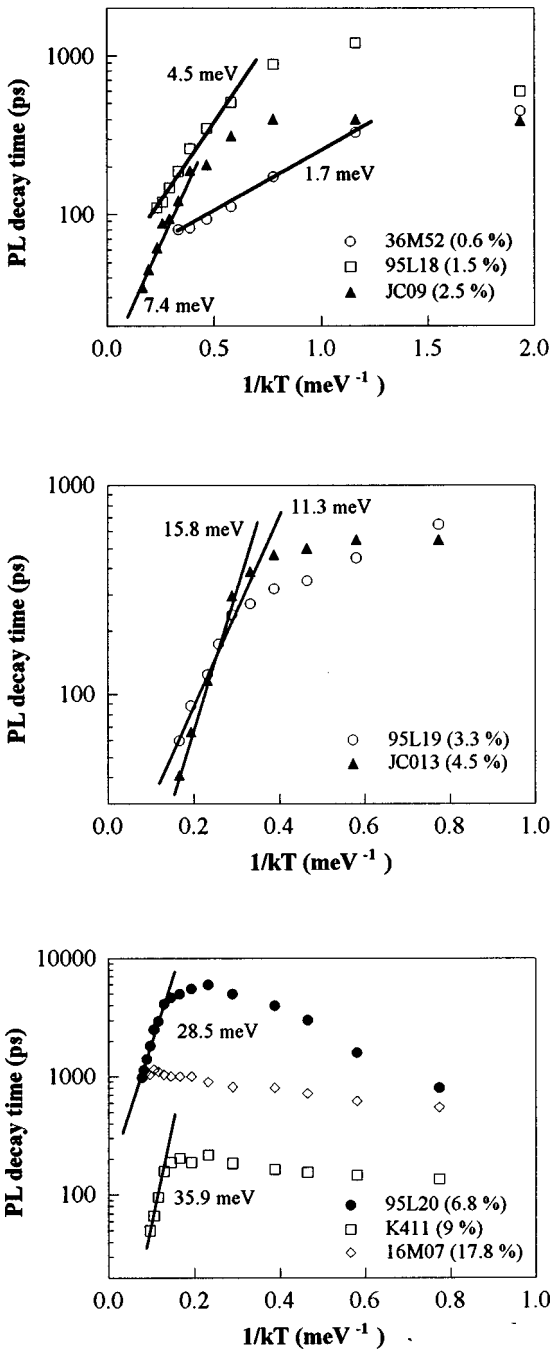

FIG. 10. Arrhenius diagram of the PL decay time for the complete set of samples. The solid lines are the best fits to the high-temperature slopes giving the activation energies for the thermally activated carrier escape.

where Δ is the effective barrier height for the escaping particle. The Arrhenius diagram is obtained by plotting $\log(\tau_{\text{nr}}) \propto \Delta/k_bT$ versus $1/T$.

In Fig. 10 we show the Arrhenius diagram for all the samples (the data point are the same as those presented in Fig. 6). An exponential law is indeed observed at high temperature, with an activation energy larger for deeper wells. We note that due to its large effective barrier height and the high quality of the sample, no activation is found in the deeper, $x=0.178$, sample. Furthermore, in the $x=0.006$

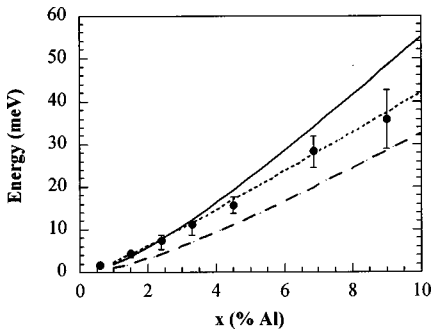

FIG. 11. Calculated effective barrier height for the electrons (solid line), heavy holes (short-dashed line), and light holes (long-dashed line) versus Al concentration. Full symbols, measured activation energies.

sample, the low effective barrier height induces a thermal escape even for very low temperature (see Sec. V B).

In order to gain insight in the microscopic origin of the thermal escape, we compared the measured activation energy with the calculated effective barrier height (Fig. 11) for the electrons, the heavy holes, and the light holes. In the figure, the error bars correspond to the inaccuracy with which the slope can be measure using Fig. 10. We observe that the activation energy is very well correlated with the effective barrier height for heavy holes. After reaching thermal equilibrium consecutive to the excitation, the radiative recombination of the fundamental state (the heavy-hole exciton) is dominated by the escape of the least confined carriers: the heavy holes. The effective barrier height for the light holes is even smaller, but (i) at thermal equilibrium the heavy holes are more numerous than the light holes, so the escape of the light holes could be statistically hidden, and (ii) the intraband relaxation from the light-hole to the heavy-hole subband is a very efficient process. Thermal escape of electron-hole pairs is unlikely responsible for the activation energies we have measured. The effective barrier height for an uncorrelated pair would be the sum of the effective barrier heights for an electron and a hole. This leads, as easily deduced from Fig. 11, to activation energies much larger than those measured. For correlated electron-hole pairs the effective barrier height is expected to be increased with respect to the one of an uncorrelated pair by the difference between the binding energies of the SQW and 3D barrier excitons. This latter quantity is always positive, leading to an activation energy larger than or at least equal to the one of the uncorrelated pair.

Finally, we compare our results with former studies. We have shown the existence of a unipolar escape mechanism of heavy holes in $GaAs/Ga_{1-x}Al_xAs$ shallow quantum wells. Our results contrast with those of Refs. 24–26, where the thermal escape of electron-hole pairs, which requires a larger activation energy, was demonstrated in $In_yGa_{1-y}As/GaAs$ QW's. Gurioli *et al.*[27] demonstrated, like we do, the thermal escape of single particles out of thin $Al_xGa_{1-x}As/GaAs$ QW's. This difference between the two systems $In_yGa_{1-x}As/GaAs$ and $Al_xGa_{1-x}As/GaAs$ is quite surprising since the band offsets seem quite similar: 57:43 (Ref. 37) and 62:38,[28] respectively.

VI. SUMMARY AND CONCLUSION

In conclusion, we have reported a study of exciton recombination dynamics in a set of eight $Al_xGa_{1-x}As/GaAs$ quantum wells, ranging from shallow quantum wells to deep conventional quantum wells, by means of photoluminescence and time-resolved photoluminescence. First, we have shown that the transition energies vary monotonically from the 2D limit to the 3D limit and can be calculated, within the experimental accuracy (0.5 meV), using a separable exciton wave function for Al concentrations as low as 0.01.

The radiative recombination time has been shown to be strongly enhanced in shallow quantum wells, compared to conventional quantum wells, mainly due to the presence of the 3D exciton gas of the barrier, which becomes closer in energy to the QW 2D exciton gas as x decreases. While a transition from the strong confinement regime to the weak confinement regime in shallow quantum wells has been predicted around $x=0.01$ (for 100-Å-wide SQW's) the predicted variation of the oscillator strength can only partly explain the experimental findings. An accurate measurement of the excitonic oscillator strength with even shallower wells is required to firmly establish the existence of the weak confinement regime.

Finally, by varying the crystal temperature, we have shown the existence of a nonradiative channel, activated at lower temperatures in shallower quantum wells. The weak excitonic binding energy in SQW's favors the thermal dissociation of excitons at very low temperatures. The microscopic origin of the nonradiative recombination following the dissociation has been revealed by studying the temperature dependence of the photoluminescence decay time. The measured activation energies have been found to agree with the unipolar escape of the carriers out of the QW's, which is a particularly efficient process in SQW's, even at very low temperatures.

ACKNOWLEDGMENTS

The Laboratoire de Physique de la Matière Condensée de l'ENS is ''Unité Associée au CNRS (URA1437) et aux Universités Paris 6 et Paris 7.'' O.H. acknowledges financial support from the EEC (TMR:ERBFMBICT 961405).

*Present address: Lawrence Berkeley National Laboratory, Material Sciences Division, 1 Cyclotron Road, MS 2-300, Berkeley CA 94720.

†Present address: Department de Fisica Aplicada, Universitat de Valencia, E-46100 Burjassot, Valencia, Spain.

[1] J. Feldmann, K. W. Goossen, D. A. B. Miller, A. M. Fox, J. E. Cunningham, and W. Y. Jan, Appl. Phys. Lett. **59**, 66 (1991).

[2] G. Von Plessen, J. Feldmann, K. W. Goossen, B. Schlichtherle, E. O. Göbel, D. A. B. Miller, and J. E. Cunningham, Semicond. Sci. Technol. **9**, 523 (1994).

[3] K. W. Goossen, J. E. Cunningham, and W. Y. Jan, Appl. Phys. Lett. **57**, 2582 (1990).

[4] K. W. Goossen, J. E. Cunningham, and W. Y. Jan, Appl. Phys. Lett. **59**, 3622 (1991).

[5] K. W. Goossen, J. E. Cunningham, M. D. Williams, F. G. Storz, and W. Y. Jan, Phys. Rev. B **45**, 13 773 (1992).

[6] J. W. Lee and D. M. Kim, IEEE J. Quantum Electron. **29**, 1393 (1993).
[7] J. Tignon, O. Heller, Ph. Roussignol, C. Delalande, G. Bastard, V. Thierry-Mieg, R. Planel, and J. F. Palmier, Appl. Phys. Lett. **72**, 1217 (1998).
[8] I. Brener, W. H. Knox, K. W. Goossen, and J. E. Cunningham, Phys. Rev. Lett. **70**, 319 (1993).
[9] M. Fritze, I. E. Perakis, A. Getter, W. Knox, K. W. Goossen, J. E. Cunningham, and S. A. Jackson, Phys. Rev. Lett. **76**, 106 (1996).
[10] A. Getter, I. E. Perakis, and S. A. Jackson, Surf. Sci. Lett. **98**, 379 (1996).
[11] P. E. Simmonds, M. J. Birkett, M. S. Skolnick, W. I. E. Tagg, P. Sobkowicz, G. W. Smith, and D. M. Whittaker, Phys. Rev. B **50**, 11 251 (1994).
[12] O. Heller, J. Tignon, J. Martinez-Pastor, Ph. Roussignol, G. Bastard, M. Maaref, V. Thierry-Mieg, and R. Planel, Nuovo Cimento D **17**, 1493 (1995).
[13] R. C. Iotti and L. C. Andreani, Phys. Rev. B **56**, 3922 (1997).
[14] T. H. Woods, C. A. Burrus, A. H. Gnauck, J. M. Wiesenfeld, D. A. B. Miller, D. S. Chemla, and T. C. Damen, Appl. Phys. Lett. **47**, 190 (1985).
[15] A. Larson, A. Yariv, R. Tell, J. Maserjian, and S. T. Eng, Appl. Phys. Lett. **47**, 866 (1985).
[16] D. A. B. Miller, Opt. Quantum Electron. **22**, S61 (1990).
[17] L. C. Andreani and A. Pasquarello, Phys. Rev. B **42**, 8928 (1990).
[18] B. Deveaud, F. Clérot, N. Roy, K. Satzke, B. Sermage, and D. S. Katzer, Phys. Rev. Lett. **67**, 2355 (1991).
[19] C. Piermarocchi, F. Tassone, V. Savona, A. Quattropani, and P. Schwendimann, Phys. Rev. B **53**, 15 834 (1996).
[20] D. Y. Oberli, J. Shah, J. L. Jewell, T. C. Damen, and N. Chand, Appl. Phys. Lett. **54**, 1028 (1989); H. J. Holland, K. Leo, K. Rother, K. Ploog, J. Feldmann, G. Peter, E. O. Göbel, K. Fujiwara, T. Nakayama, and Y. Otha, Phys. Rev. B **38**, 7635 (1988); B. Deveaud, J. Shah, T. C. Damen, and W. T. Tsang, Appl. Phys. Lett. **52**, 1886 (1988); M. R. X. Barros, P. C. Becker, D. Morris, B. Deveaud, A. Regreny, and F. Beisser, Phys. Rev. B **47**, 10 951 (1993).
[21] J. A. Brum and G. Bastard, Phys. Rev. B **33**, 1420 (1986); Y. Marayama, *ibid.* **34**, 2500 (1986); J. A. Brum, T. Weil, J. Nagle, and B. Vinter, *ibid.* **34**, 2381 (1986).
[22] O. Heller and G. Bastard, Phys. Rev. B **54**, 5629 (1996).
[23] H. Hillmer, A. Forchel, T. Kuhn, G. Malher, and H. P. Meier, Phys. Rev. B **43**, 13 992 (1991); M. Krahl, D. Bimberg, R. K. Bauer, D. E. Mars, and J. N. Miller, J. Appl. Phys. **67**, 434 (1990); P. K. Basu and P. Ray, Phys. Rev. B **44**, 1844 (1991).
[24] M. Vening, D. J. Dunstan, and K. P. Homewood, Phys. Rev. B **48**, 2412 (1993); J. R. Botha and A. W. R. Leitch, *ibid.* **50**, 18 147 (1994); P. Michler, A. Hangleiter, M. Moser, M. Geiger, and F. Scholtz, *ibid.* **46**, 7280 (1992).
[25] J. D. Lambkin, D. J. Dunstan, K. P. Homewood, L. K. Howard, and M. T. Emeny, Appl. Phys. Lett. **57**, 1986 (1990).
[26] G. Bacher, C. Hartmann, H. Schweizer, T. Held, G. Malher, and H. Nickel, Phys. Rev. B **47**, 9545 (1993).
[27] M. Gurioli, J. Martinez-Pastor, M. Colocci, C. Deparis, J. Massies, G. Neu, A. Bosacchi, and S. Franchi, Phys. Rev. B **44**, 3115 (1991).
[28] In order to deduce the Al concentration, we used the formula $E_g(\mathrm{Al}_x\mathrm{Ga}_{1-x}\mathrm{As}) = (1519.2 + 1250x)$ meV, as given by E. T. Yu, J. O. McCaldin, and T. C. McGill, *Solid State Physics*, edited by H. Ehrenreich and D. Turnbull (Academic Press, San Diego, 1992), Vol. 46, pp. 2–146, and assumed a 4-meV excitonic binding energy for the 3D barrier material.
[29] G. Bastard, E. E. Mendez, L. L. Chang, and L. Esaki, Phys. Rev. B **26**, 1974 (1982).
[30] Nguyen Hong Ky, J. D. Ganière, M. Gailhanou, F. Morier-Genoud, D. Martin, and F. K. Reinhart, Phys. Rev. B **46**, 6947 (1992).
[31] J. E. Fouquet and A. E. Siegman, Appl. Phys. Lett. **46**, 280 (1985).
[32] G. Bastard, *Wave Mechanics Applied to Semiconductor Heterostructures* (Les Editions de la Physique, Paris, 1988).
[33] M. Gurioli, A. Vanittieri, M. Colocci, C. Deparis, J. Massies, G. Neu, A. Bosacchi, and S. Franchi, Phys. Rev. B **44**, 3115 (1991).
[34] H. W. Liu, C. Delalande, G. Bastard, M. Voos, G. Peter, R. Fisher, E. O. Göbel, and J. A. Brum, Phys. Rev. B **39**, 13 537 (1989).
[35] H. J. Polland, L. Schultheis, J. Kulh, E. O. Göbel, and C. W. Tu, Phys. Rev. Lett. **55**, 2610 (1985); J. Aaviksoo, C. Gourdon, R. Grousson, P. Lavallard, and R. Planel, Solid-State Electron. **40**, 687 (1996).
[36] L. C. Andreani, Phys. Scr. **T35**, 111 (1991).
[37] B. Soucail, N. Dupuis, R. Ferreira, P. Voisin, A. P. Roth, D. Morris, K. Gibb, and C. Lacelle, Phys. Rev. B **41**, 8568 (1990).